ECSE-529A
Image Processing and Communication

Project Report

Removing Shadows from Images

by

Samuel Audet

December 2, 2005

ECSE-529A

Image Processing and Communication

Instructor: M. D. Levine

Project Report

Removing Shadows from Images

by

Samuel Audet
saudet@cim.mcgill.ca
ID: 260184380

December 2, 2005

Electrical and Computer Engineering Department
3480 University Street Room 410
Montreal, Quebec
Canada H3A 2A7

ABSTRACT

Removing Shadows from Images

Samuel Audet

For this project, the shadow removal method used by Finlayson et al. in [1] was implemented. This report contains an overview of the mathematical background and a detailed discussion on the experiments performed with the implementation.

This method consists of two independent steps. First, an illumination invariant image is derived from a color image for which an appropriate color calibration is known. Second, shadow edges are detected by finding edges in the intensity image that are not in the illumination invariant image. Gradient information is then erased at those shadow edges, and a new shadowless color image is formed by solving a Poisson's equation.

ACKNOWLEDGMENTS

I would like to thank Professor Martin D. Levine for teaching the Image Processing course from which I learned a lot of interesting material. I also gratefully acknowledge help received from Stéphane Pelletier and Professor Paul Tupper with regards to understanding some of the mathematical background. Thanks as well to Jonathan Miller for proofreading this report.

Contents

List of Figures

Chapter 1

Introduction

Shadows have always plagued computer vision applications where tracking, segmentation, detection and recognition algorithms confuse the boundaries of shadows with those of different surfaces or objects. It is therefore of great interest to discover ways of properly detecting shadows and removing them while leaving other details of the original image untouched. The ideal shadowless image would be an image where, although shading occurs due to the texture of the material, large patches of shadows are removed, effectively taking out the direction of the illumination, and leaving only the reflectance and the locally shaded texture. It is this goal that the shadow removal method of Finlayson et al. [1] attempts to achieve.

For this project, the shadow removal method of Finlayson et al. was implemented, and experiments were conducted. However, before discussing the results of those experiments, first a literature review providing an overview of other methods used to achieve similar goals are briefly explained and critically evaluated with regards to their advantages and disadvantages. Then, the theoretical background of the method of interest in this report is briefly explained. It is composed of two independent steps. The first step consists in deriving an illumination invariant image from a color image. This step requires the knowledge of a color calibration appropriate to this method. In the second step, the shadow edges are detected and used to produce a new gradient image which is integrated by solving the Poisson's equation to recover the new shadowless color image. Finally, experimental results showing how close the method is at achieving its goal are discussed while detailing its capabilities and limitations for both test images and real world images. Although in some cases the method offers acceptable results, it is far too sensitive to busy images, images where the Planckian lighting assumption does not hold, or camera sensors whose responses are not sufficiently narrow. The method also fails to remove shadows with very smooth edges.

Chapter 2

Literature Review

A lot of research on shadow detection has been performed, but not as much was done on shadow removal. The interest of shadow removal is not limited to the detection of the shadow. It is also sometimes important to find ways to remove the effect of the shadow while still keeping the underlying texture of the surfaces. For example, in applications where both tracking and recognition of objects are important, one would might wish to keep the shading of textured surfaces intact, while discounting the effect of sharp shadows casted upon those surfaces.

Work by Weiss in [2] demonstrates how to recover intrinsic illumination and reflectance images under the assumption that the histogram of the illumination and intensity derivatives are sparse, meaning most of the values are 0. A sequence of images with illumination changes, where shadow edges move, but with no reflectance changes, where all the surfaces and objects do not move, go through derivation filters. For each pixel, only the median of this sequence is kept, amounting to the maximum-likelihood estimation of the invariant reflectance. While this method computes very natural looking, shadowless images, it does not work on single images, or on a sequence where illumination does not change or where the reflectance does.

Levine et al. in [3] show a method making various assumptions about the behavior of shadows at their boundaries, and segment images into shadow and non-shadow regions with the help of a manually trained support vector machine. After some post-processing, continuous and closed boundaries are found, and pixel color within the shadow regions are replaced with the average color found at the boundaries. Unfortunately, this method removes all high frequency details from the shadow regions and amounts to a very strong smoothing of the reflectance.

The goal of work done by Sasagawa et al. in [4] is to remove shadows from satellite images where geometric information of the scene and of the light source, the sun, are known. A model of casted shadows can thus be precomputed with this knowledge, but it is impractical for general purposes where no geometric information is known.

Tappen et al. in [5] build derivative images of the "shading" (gray-scale illumination) and of the reflectance. They use a color classifier based on the invariance properties of normalized RGB and a manually trained grayscale classifier based on a local analysis of edges with the help of the AdaBoost algorithm to find optimal filters and thresholds. The resulting derivatives are then integrated in the same way as in [2], giving quite good results. This method, however, tends to remove a lot of texture information from the reflectance image.

The ShadowFlash algorithm [6] effectively removes shadows from scenes in an active manner by illuminating an object or a scene from several different angles. Although it produces very good results, it is an active technique and is not applicable to images in general.

Chapter 3

Shadow Removal Theory

Two independent steps are involved in the shadow removal method of Finlayson et al. [1]. The first step consists in performing operations to get an illumination invariant image, which is a grayscale representation proportional to the color reflectance of the surfaces. To work properly, this step requires some color calibration as well as other conditions described below. The second step consists in finding shadow edges and removing them from the color image. Shadow edges are defined as edges that are part of the intensity image, but not of the illumination invariant image. With these shadow edges, it is possible to stamp these edges off from the gradient of each color channel, and to recover a shadowless color image by solving a linear system approximating the Poisson's equation to integrate the now shadowless image from the modified gradient information.

To produce the illumination invariant image, there are a few assumptions made. First, a color calibrated camera whose sensor responses are directly proportional to the luminance is used (but it will be shown that a more loosely defined calibration is sufficient); second, the scene is illuminated with Planckian lighting; third, the sensor responses of the camera are fairly narrow. To understand how this procedure works, recall that the intensity measured by a sensor is given by

$$\rho_k = \int E(\lambda)S(\lambda)Q_k(\lambda)d\lambda \text{ where } k = R, G, or B, \tag{3.1}$$

and $E(\lambda)$ is the spectral power distribution of the illumination, $S(\lambda)$ is the surface reflectance distribution, and $Q_k(\lambda)$ is the sensor sensitivity distribution. If the sensor response is narrow enough, it can be approximated by a Dirac delta function: $Q_k(\lambda) \approx q_k\delta(\lambda - \lambda_k)$, where $q_k = Q(\lambda_k)$ is the maximum response of the sensor at λ_k. Therefore,

$$\rho_k \approx E(\lambda_k)S(\lambda_k)q_k. \tag{3.2}$$

Moreover, assume the lighting can be approximated by Planck's law:

$$E(\lambda) = \frac{I2hc^2}{\lambda^5}\frac{1}{e^{\frac{hc}{\lambda kT}} - 1} \tag{3.3}$$

where T is the temperature of the black body, h is Planck's constant, c is the speed of light, k is Boltzmann's constant, and I a factor representing the incident intensity of the light. Through manipulation of equations (3.2) and (3.3) with three intensities from the three color channels, one can demonstrate [1] that

$$gs = c_1 \ln \frac{\rho_R}{\rho_G} - c_2 \ln \frac{\rho_B}{\rho_G} \text{ where } c_1 = \frac{1}{\lambda_B} - \frac{1}{\lambda_G} \text{ and } c_2 = \frac{1}{\lambda_R} - \frac{1}{\lambda_G} \tag{3.4}$$

is illumination invariant and solely depends on the reflectance of the surface. In this representation, big numbers in absolute value tend to represent colorful surfaces, and colorless surfaces (white, gray and black) tend to have lower values.

The second step consists of stamping out the border of the shadows, which are called shadow edges. The SUSAN edge detector [7] is used to find those shadow edges. The edge detector first blurs the image using a Gaussian kernel of given parameter σ, and then runs the SUSAN thresholding operation. Only the strongest edges are kept, and no other operations from the SUSAN algorithm are performed. Any edges found in the intensity image $I = (R + G + B)/3$ not found in the illumination invariant image are assumed to be shadow edges. Small noisy edges are eliminated with a morphological opening operation. Due to the penumbra, shadow edges are not always sharp [3], so a thicker edge representation is required. To accomplish this, a morphological dilation operation is used to thicken the shadow edges.

Next, taking the gradient of the image in the log domain and setting pixels corresponding to shadow edges to 0 effectively stamps out those edges. The reason this works is because, according to equation (3.2), if one makes the assumption that $S(\lambda)$, the reflectance, does not change (which means the shadow is casted within the surface boundaries), then what is left after taking the finite difference of two such log-domain pixels (done as part of the gradient computation) is the difference in illumination $E(\lambda)$. This is akin to lightness recovery methods. The shadow edges thus drive the following algorithm :

$$\nabla sl'(x, y) = \begin{cases} 0 & \text{if } se(x, y) > 0 \\ \nabla \rho'(x, y) & \text{otherwise} \end{cases} \tag{3.5}$$

where $sl'(x, y)$ is the shadowless image in the log domain, $se(x, y)$ are the shadow edges, and $\nabla \rho'(x, y) = \nabla \ln \rho(x, y)$. This gradient is approximated by convolution with masks $\begin{bmatrix} 1 & 0 & -1 \end{bmatrix}$ for ∇_x and $\begin{bmatrix} -1 & 0 & 1 \end{bmatrix}^T$ for ∇_y. This procedure therefore removes the difference in illumination at shadow edges, if the invariant reflectance assumption holds. This is done for the three color channels separately.

After which the image is reintegrated by first computing the Laplacian of $sl'(x, y)$ by taking the gradient of $\nabla sl'(x, y)$, and by then solving the Poisson's equation:

$$\nabla^2 sl'(x, y) = \nabla \cdot (\nabla sl'(x, y)) \tag{3.6}$$

using Neumann boundary conditions for which the derivative is zero. This returns $sl'(x, y)$, the image in the log domain of the desired shadowless image, up to an unknown additive constant. The Neumann condition is used so shadows that extend to the edges of the image are not pulled back to their original dark shadow values. However, due to the same Neumann boundary condition, each value is only exact up to an unknown additive constant. Taking the exponential $e^{sl'(x,y)+k_1} = k_2\ sl(x, y)$, this translates into an unknown multiplicative constant. To compensate for this loss of information, for a given channel, each pixel value is divided by the average of the pixel values belonging to the top first percentile. This usually produces good results. However, in this report instead of the average, the median is used, as it proved to give better results for the input images studied.

To summarize and clarify the operations of the algorithm, here is a detailed description of each parameter.

- c_1 and c_2 are the constants used to create the illumination invariant image, and are also related to the color calibration of the camera. Once these values are established for a given camera, they do not need to be readjusted. Moreover, the author goes on to prove that one does not need a color calibrated camera to find working constants, and that a working calibration step for the algorithm can consist of a sequence of images of a scene taken under varying lighting intensities, such as an outdoor scene over a period of a few hours [1].

- σ represents the standard deviation of the Gaussian kernel used for the smoothing operation before shadow edge detection. Noisy images or images with a lot of high-frequency details need a higher value. Usual values range from 1 to 7.

- t_1 is the SUSAN threshold for the intensity image. In the ideal case, the resulting intensity edges must include all shadow edges. Usual values range from 5 to 20.

- t_2 is the SUSAN threshold for the illumination invariant image. In the ideal case, these edges must contain all edges from the intensity edges, while not containing any shadow edges. Usual values range from 5 to 20.

- r_1 is the radius of the structuring disk element for the morphological opening operation on the shadow edges. It should be set to the size of small noisy edges in an attempt to erase them, while keeping real shadow edges. Usual values range from 1 to 3.

- r_2 is the radius of the structuring disk element for the morphological dilation operation on the shadow edges. It should be set to the width of real shadow edges in an attempt to completely remove them from the gradient. Usual values range from 3 to 10.

Chapter 4

Experimentation and Discussion

To demonstrate how the algorithm functions and explain its capabilities and limitations, the output produced from a few artificial test images are first discussed. Following this, results from real world images are shown and discussed. For display and printing purposes, processed images are all converted back to the sRGB color space [8], which consists of applying a gamma correction of 2.2 on images whose values are linearly related to the luminance.

4.1 Artificial Test Images

The first artificial test image as shown in figure 4.1(a) consists of an almost pure blue background and four ellipses which represent different kinds of situations the algorithm might face. The top first ellipse is a ”perfect shadow” in the sense that the pixel values are uniform across the ellipse, that the shadow edge is very sharp, and that its illumination invariant value is the same as the background. The second one is an extremely smoothed version of the first which results in a much more spread out shadow edge. The illumination invariant value remains unchanged since the shadow edge is now merely a linear combination of two colors that produce the same invariant value. The third one is a slightly greener and redder shadow, which to the naked eye is pretty similar to the first. Nonetheless, this corresponds to

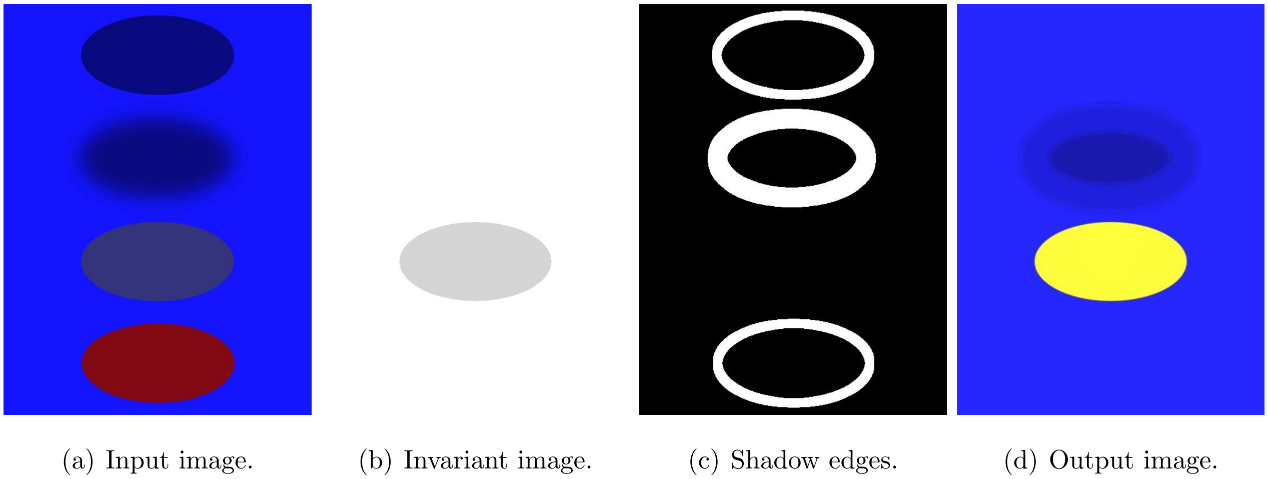
(a) Input image. (b) Invariant image. (c) Shadow edges. (d) Output image.

Figure 4.1. First test image processed with $\sigma = 3$, $t_1 = 5$, $t_2 = 5$, $r_1 = 1$, $r_2 = 3$

the case of a bad calibration or a failure of the Planckian lighting assumption. The invariant value for this case is thus different, as seen in figure 4.1(b) . The last ellipse consists of a completely different color producing the same invariant value. This ellipse is a model of a surface having different reflectance than the background, but which maps to the same invariant value. This is an inherent limitation of the method. One can easily show from equation (3.4) that the information from the red and blue channels is effectively summed up, so it is always possible to inverse the values of these two channels, in accordance with the calibration, without changing the invariant value. The algorithm is in effect red/blue color-blind.

In the output image (figure 4.1(d)), as expected, the first ellipse has completely disappeared. The second one is partially attenuated, but one can see from the shadow edges in figure 4.1(c) that the its shadow edge is not thick enough. It can be successfully removed by increasing the parameter r_2 thus increasing the width of the shadow edge, as seen in figures 4.2(c) and 4.2(d). However, increasing the morphological dilation of shadow edges to big values will erase more gradient information found within the shadow edge. This loss of information shows up as smearing marks in natural images as seen below. The third ellipse was not removed because it produced no shadow edge, but moreover the green channel is severely amplified, resulting in discoloration. This problem occurs because of the normalization performed to estimate the unknown multiplicative constant after integrating the gradient with Neumann boundary conditions. In the input image (figure 4.1(a)) the values of the green channel are very low overall, while the highest value is found within the third ellipse. After

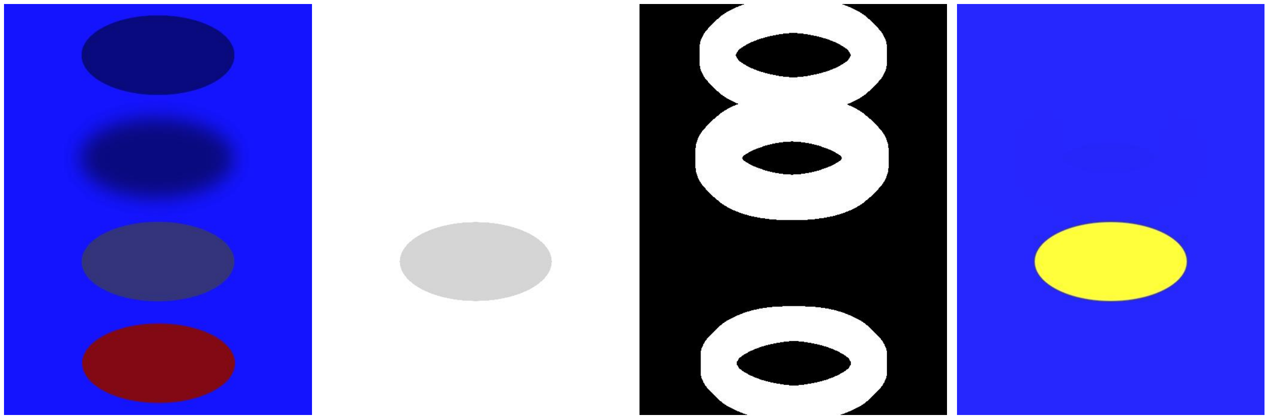

(a) Input image. (b) Invariant image. (c) Shadow edges. (d) Output image.

Figure 4.2. First test image processed with $\sigma = 3$, $t_1 = 5$, $t_2 = 5$, $r_1 = 1$, $r_2 = 24$

integration, the algorithm simply takes the highest green value and maps it to the highest pixel value possible. Now the green in the third ellipse comes out with the brightest possible value. Next, since this algorithm is red/blue color-blind, it comes to no surprise that the fourth ellipse is completely gone the same way the first one was removed. However, in this case, it is a false positive as it does not represent an actual shadow.

The second test image (figure 4.3(a)) models a very busy background with a shadow edge running over it. As one can see in the invariant image (figure 4.3(b)), the shadow is properly ignored and all the busy information is not discarded. Everything is fine up until the point where shadow edges are located, figure 4.3(c). It is a disaster. The real shadow edge is not retained and many spurious edges from the busy background crop up. The reason for this is that, in addition to the shadow edges, the edges detected in the intensity image and the ones detected in the invariant image are not exactly the same. The gradients of both images vary differently, and thus the pixels of the edges do not have a one to one correspondence. The

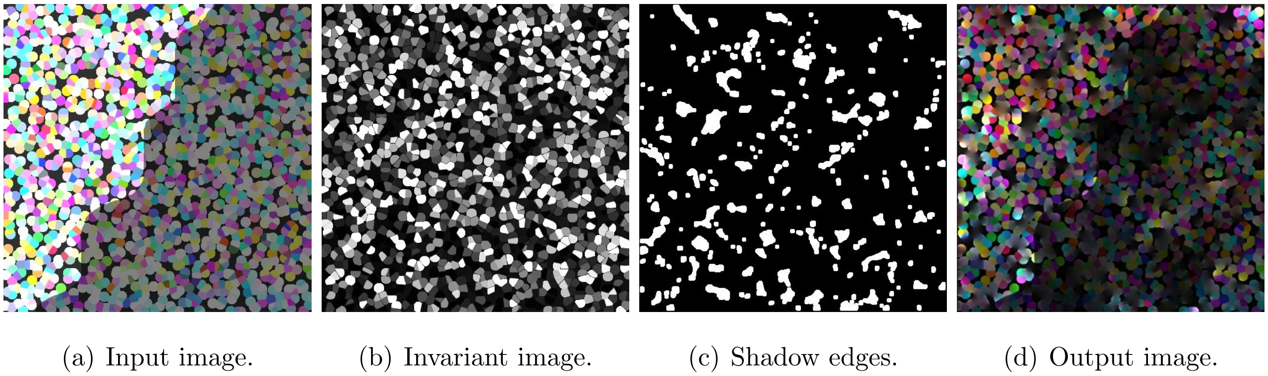
(a) Input image. (b) Invariant image. (c) Shadow edges. (d) Output image.

Figure 4.3. Second test image processed with $\sigma = 3$, $t_1 = 5$, $t_2 = 5$, $r_1 = 1$, $r_2 = 3$

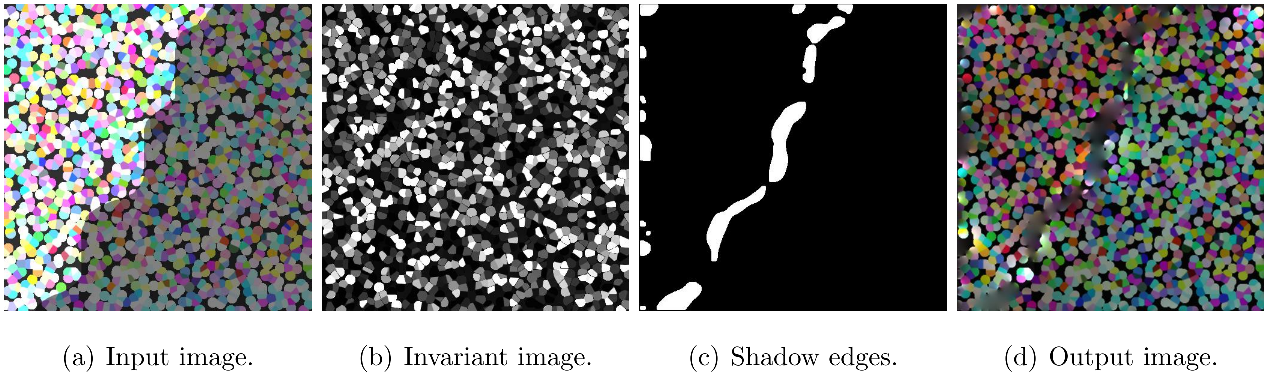
(a) Input image. (b) Invariant image. (c) Shadow edges. (d) Output image.

Figure 4.4. Second test image processed with $\sigma = 15$, $t_1 = 5$, $t_2 = 5$, $r_1 = 1$, $r_2 = 3$

shadow edge is found somewhere in the middle of this mess and it is erased, since it passes on top of actual reflectance changes in the invariant image, hence the misclassification. To compensate for such images, one has to increase the σ value associated with the smoothing operation. With a value of 15, the shadow edge can be located with some success, as shown in figure 4.4(c). Such intensive smoothing can, however, make shadow edges disappear in other types of images where shadow regions are narrow.

The implementation is behaving as expected with these artificial test images so it is believed to work properly. For further discussion on the method, in the next section, it is tested with real world images.

4.2 Real World Images

For experiments with real world images, images from the McGill Calibrated Colour Image Database [9] were used. The use of these already-calibrated images removed the burden of calibration and facilitated work on the algorithmic aspects of the problem. More information on color calibration can be found in the documentation at this site. From this documentation, the peak sensor responses of the cameras used to take these pictures are $\lambda_B = 470$ nm, $\lambda_G =$ 530 nm, and $\lambda_R = 590$ nm. From equation (3.4): $c_1 = 0.24 \times 10^{-12}$ and $c_2 = -0.19 \times 10^{-12}$, or after normalization: $c_1 = 0.78$ and $c_2 = -0.62$. Since the sensor responses are obviously not Dirac delta functions, these values were taken as initial approximations of the optimal values. After visually evaluating a range of values and the resulting invariant images, it was found that the values $c_1 = 0.47$ and $c_2 = -0.67$ gave the best results, and so these are the values that were used for all the images.

Starting with merry0101.tif in figure 4.5, the first prominent issue is that the invariant image really is not that invariant, which is obvious when looking at the shadow edges in the invariant image. In the original paper [1], the invariant images look illumination invariant, but it does not seem to work as well with the pictures used in this report. This indicates that the narrow sensor response approximation assumed for equation (3.2) does not hold as well as expected. Moreover, the noise pattern in the dark area is different from the one in the bright area. Nonetheless, even in this situation it is possible to obtain relatively good results. The shadow edges of figure 4.5(c) and the output (figure 4.5(d)) are quite acceptable. However, there are a few things to notice about the output image. First, the overall color is different. This is due to the Neumann boundary conditions and the subsequent per-channel normalization. Second, as indicated before, the portion of the gradient erased at the shadow

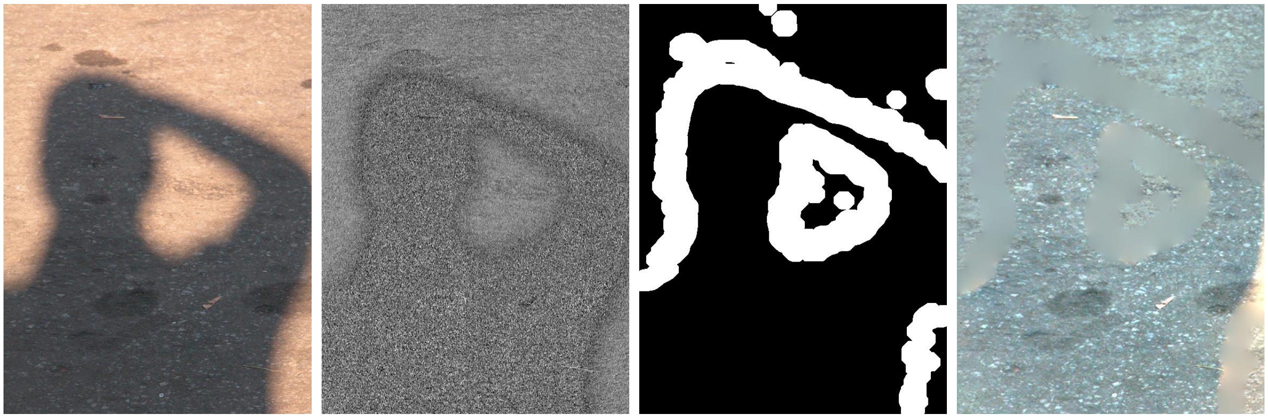

(a) Input image. (b) Invariant image. (c) Shadow edges. (d) Output image.

Figure 4.5. merry0101.tif processed with $\sigma = 5$, $t_1 = 5$, $t_2 = 10$, $r_1 = 2$, $r_2 = 15$

edges appear as smearing marks in the output image. It is assumed the reflectance does not change when executing equation (3.5), but the reflectance does in fact change as this is textured dirt, and the information about this texture is smoothed out, resulting in visible smearing marks. Also, the shadow is not completely removed since the edge detector fails to properly locate the edges in the lower right corner of the picture. Should it detect them properly, the overall color and intensity of the image would be constant. This not being the case, some of the original gradient information is kept, affecting the whole image, albeit the farther away a pixel is from the error, the smaller the effect. This can be explained by an analysis of the conditioning of the problem. The condition number of the matrix for approximating the Laplacian and for solving the Poisson's equation (3.6) over a square image of resolution 512×512 is estimated to be 15×10^4, which robs the results of a maximum of $\log_{10}(15 \times 10^4) = 5.2$ digits of accuracy in the worst case. The solutions shown in this report were computed using IEEE 754 double precision floating-point arithmetic, which provides $-\log_{10}(2^{-52}) = 15.7$ digits of accuracy. This demonstrates that the problem is well-posed and not very sensitive to noise, which in this case is mainly created when manipulating the gradient images. This well-conditioned system provides robustness to failure.

Figures 4.6 and 4.7 are very complex images that cannot be properly processed as a whole. The busy pattern created by the leaves and the grass produces a lot of noisy edges and interferes with the localization of shadow edges. The shadow edges on the grass or in the leaves do not come out very cleanly or at all, as seen in figures 4.6(c) and 4.7(c). It would be possible to use stronger smoothing to compensate. However, in this case the gist of the shadows in these images, consisting of narrow shadows, would be smoothed out and

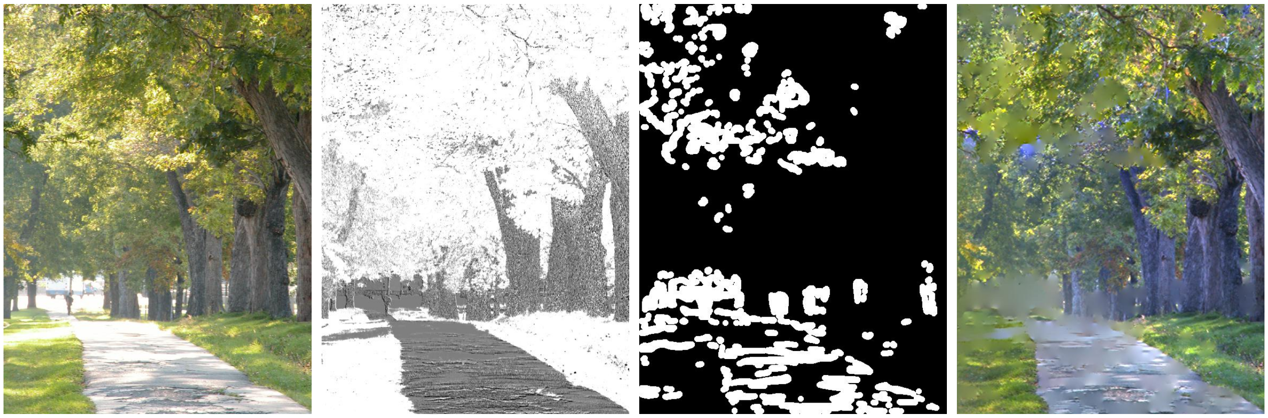

(a) Input image. (b) Invariant image. (c) Shadow edges. (d) Output image.

Figure 4.6. merry0107.tif processed with $\sigma = 3$, $t_1 = 15$, $t_2 = 15$, $r_1 = 1$, $r_2 = 5$

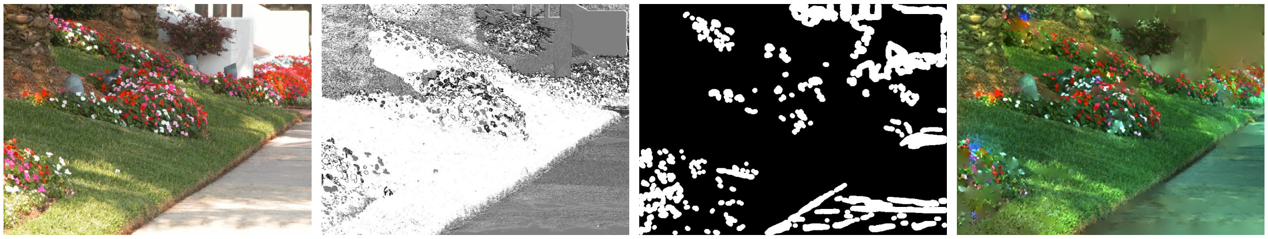

(a) Input image. (b) Invariant image. (c) Shadow edges. (d) Output image.

Figure 4.7. merry_florida0005.tif processed with $\sigma = 3$, $t_1 = 15$, $t_2 = 15$, $r_1 = 1$, $r_2 = 5$

not detected. Therefore, the results shown in figures 4.6(d) and 4.7(d) are about the best that can be achieved with this technique. Also notice the blue halos pouring out of some of the leaves and flowers. The blue channel being the noisiest channel is most sensitive to changes. The maximum value of the Laplacian of this channel is usually 3 to 4 times higher than what is observed from the red and green channels. Abruptly modifying these values as done by this method thus results in larger errors in this channel.

In contrast, figures 4.8 and 4.9 are images for which this procedure works well. The images are not very busy and the shadow edges are sharp and well located by the edge detector. It is still not perfect, and one can notice the slight discoloration. Also note that in figure 4.9 there is a lot of shadows around the sculptures at the top. In this case, one would actually wish to keep these shadows intact, as they offer information about the shape of the sculptures, which is lost in the shadowless image, as seen in the output image, figure 4.9(d).

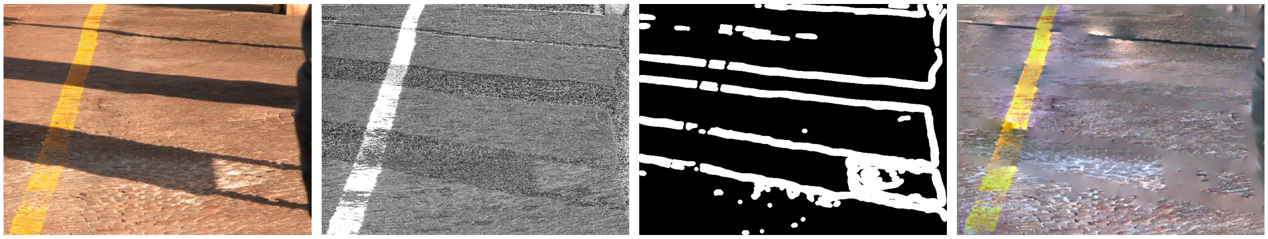

(a) Input image. (b) Invariant image. (c) Shadow edges. (d) Output image.

Figure 4.8. merry_italy0146.tif processed with $\sigma = 5$, $t_1 = 7$, $t_2 = 10$, $r_1 = 1$, $r_2 = 5$

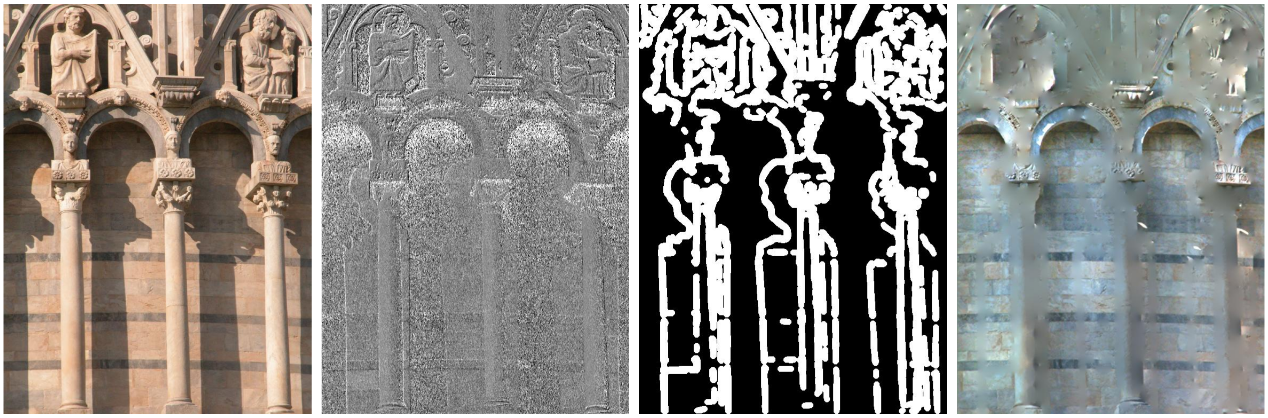

(a) Input image. (b) Invariant image. (c) Shadow edges. (d) Output image.

Figure 4.9. merry_italy0188.tif processed with $\sigma = 3$, $t_1 = 15$, $t_2 = 10$, $r_1 = 1$, $r_2 = 5$

A real world example of the second test image of figure 4.3 is figure 4.10, where a grass lawn is partially covered by shadows. To effectively locate the shadow edges, a very strong smoothing must be applied. A σ of 7 does the trick, and shadow edges are locate with some success. The undetected shadows are too narrow and are smoothed out. With this imperfect representation of shadow edges, it is still possible to recover a good image with less shadows than the input image, as seen in figure 4.10(d). Notice again noisy blue pixels coming out in the resulting image. As discussed before, the blue channel, being the noisiest channel, is where errors tend to grow more.

Figure 4.11 is an example where a shadow edge is too smoothed out, or in other words where the penumbra is too important. In this case, it is impossible for the edge detector to ever detect the contour of this shadow, even by adjusting parameters to their extremes. The method only works well with sharp shadows. Even if it were possible to detect these shadow edges properly, a very strong thickening by increasing parameter r_2 would be needed to

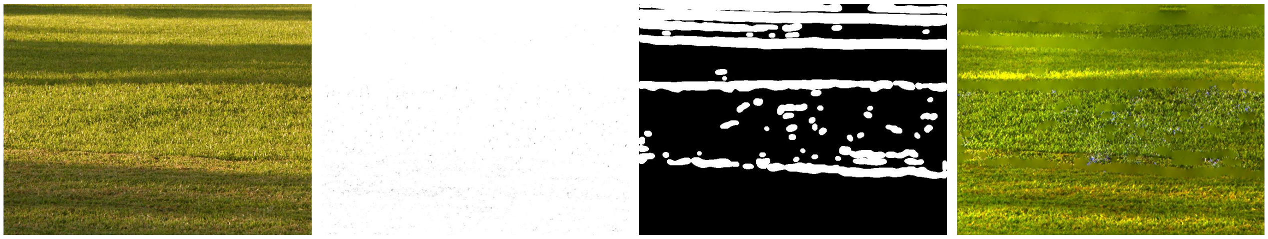

(a) Input image. (b) Invariant image. (c) Shadow edges. (d) Output image.

Figure 4.10. merry_mexico0140.tif processed with $\sigma = 7$, $t_1 = 3$, $t_2 = 7$, $r_1 = 1$, $r_2 = 5$

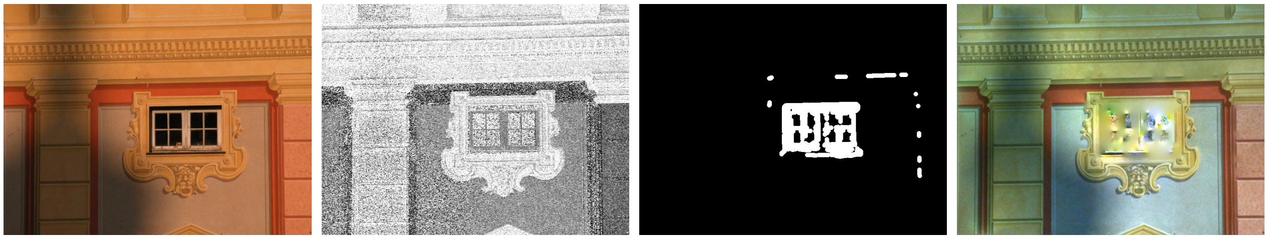

(a) Input image. (b) Invariant image. (c) Shadow edges. (d) Output image.

Figure 4.11. merry_italy0052.tif processed with $\sigma = 3$, $t_1 = 15$, $t_2 = 15$, $r_1 = 1$, $r_2 = 5$

properly remove the shadows, which would cause a lot of collateral damage to the shadowless image.

Another case where this technique works well is for snow, as shown in figure 4.12. Snow is a very soft material, in general, so few edges interfere with shadow edges. Most of the shadows are successfully removed with little trouble, as seen in the output image, figure 4.12(d). However, there is something odd at the top right corner of the output image. A bright patch of white surrounded by colorful pixels and pseudo-rays of light. This area is ”connected” to a lot of the image by only its shadow edges, figure 4.12(c). When solving the Poisson’s equation, in order to satisfy all the null gradients, the values in this area shoot up and create this anomaly that is not bound at the border to any specific values, due to the Neumann boundary conditions. However, at the same time these effects are localized and do not affect large image portions, thanks to the stability of the numerical solution as demonstrated before.

As a final note, the thresholds t_1 and t_2 were not discussed for the experiments. A threshold t_1 that seems to let through all the shadows edges of the intensity image has to be determined manually. Then, one must find t_2 such that the edge detector can find edges in

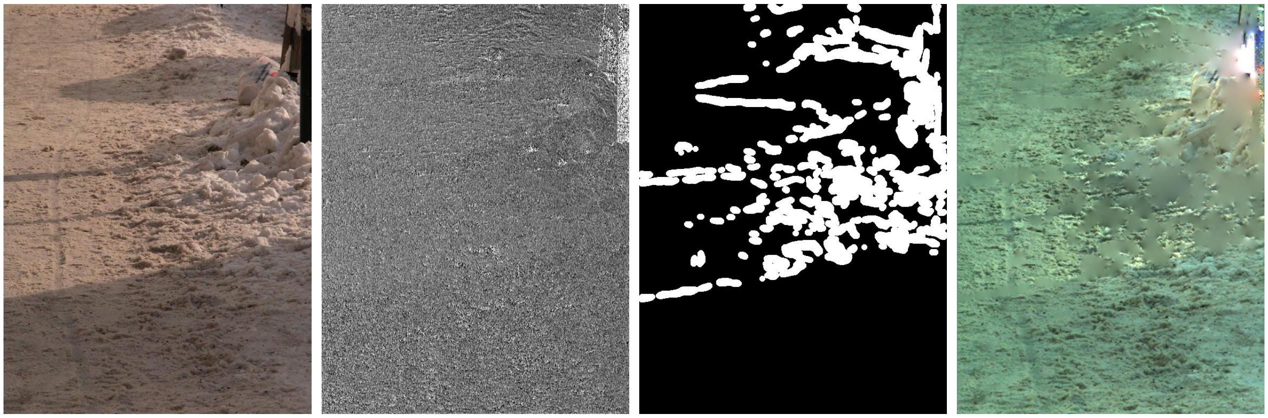

(a) Input image. (b) Invariant image. (c) Shadow edges. (d) Output image.

Figure 4.12. merry_winter0033.tif processed with $\sigma = 5$, $t_1 = 5$, $t_2 = 10$, $r_1 = 1$, $r_2 = 5$

the invariant image which would ideally include all the edges in the intensity image except shadow edges. However, fixing these parameters is a very subjective and error prone trial-and-error procedure. In general, good thresholds rarely exist, and detected shadow edges always contain a large amount of unwanted edges while real shadow edges are often broken or not detected. Also, variation of the parameter r_1 does not appear to help a lot in removing noisy edges without damaging the shadow edges, and so was almost entirely ignored of the discussion for this reason.

Chapter 5

Conclusion

In this report the shadow removal method by Finlayson et al. [1] was briefly explained, and using an implementation of this method, experiments were conducted and a discussion clarifying the results was given.

This method [1] consists of first deriving an illumination invariant image under the assumptions of a color calibrated camera and of Planckian illumination. It was also seen that a color calibrated camera was not necessary, and a more loosely defined calibration obtainable from a sequence of images of a scene under varying illumination was sufficient. Second, edge detection using the SUSAN algorithm is performed on both the intensity image and the illumination invariant image to find shadow edges. Any edges found in the intensity image but not in the invariant image are considered to be a shadow edges. Gradient information in the log domain corresponding to illumination changes is removed from the image by setting to 0 the magnitude of the gradient at pixels belonging to a thickened version of these shadow edges. The new shadowless image is then integrated from this modified gradient.

Apart from the requirements of color calibration and Planckian lighting, there are a few other problems with this shadow removal method. First, the sensor response of the camera must be sufficiently narrow to provide a good illumination invariant image, although work done in [10] to compensate for sensors with a broad spectrum looks promising. Second, the illumination invariant image is red/blue color-blind, which can possibly lead to incorrectly classified edges. Third, it is hard for the algorithm to work properly when shadow edges fall on reflectance edges as well. This situation is common in busy natural images. Another problem arises because gradient magnitude is simply set to 0 at the shadow edges. It is assumed the reflectance does not change when executing equation (3.5), but the reflectance does in fact often change, and the information about it is distorted, resulting in visible smearing marks. These marks are especially visible when very spread out shadow edges need to be covered up. This could be compensated for by detecting the direction of the shadow edges as well and nullifying only that direction. Next, when these edges are too spread out, they are not even detected. This method is only effective for sharp shadow edges. Also, due to the Neumann boundary conditions, the resulting shadowless image often suffers from discoloration. It should however be possible to bind the color channels together in a way that their relative values are restored. Finally, taking the gradient of the gradient to solve the Laplacian introduces a lot of unnecessary errors. It would be better to solve for the shadowless image directly from the gradient. Moreover, before taking the gradient, it might not even be necessary to switch to the log domain and also avoid the errors produced by this calculation.

In conclusion, this method does not seem to be very useful on its own. In addition to the inherent technical limitations of the method, it does not appear to produce clean enough results appropriate for further analysis with other computer vision algorithms or appropriate for human consumption, as the results are not visually pleasing as well. In light of the results obtained in [3] and [5], it seems obvious that a trained classifier is better than a simple edge detector at splitting information related to illumination from information related to reflectance. It is rarely possible to find good thresholds for the edge detector to detect shadow edges without incorporating various other edges. It should be possible to elaborate an algorithm based on these two methods and the method detailed in this report that would give better results than the ones obtained by any of those algorithms at the moment.

References

[1] G. D. Finlayson, S. D. Hordley, and M. S. Drew, "Removing Shadows from Images," in *ECCV '02: Proceedings of the 7th European Conference on Computer Vision-Part IV*, (London, UK), pp. 823–836, Springer-Verlag, 2002.

[2] Y. Weiss, "Deriving Intrinsic Images from Image Sequences.," in *ICCV*, pp. 68–75, 2001.

[3] M. D. Levine and J. Bhattacharyya, "Removing shadows.," *Pattern Recognition Letters*, vol. 26, no. 3, pp. 251–265, 2005.

[4] Y. Li, T. Sasagawa, and P. Gong, "A system of the shadow detection and shadow removal for high resolution city aerial photo," in *Proceedings Volume of the Geo-Imagery Bridging Continents, XXth ISPRS Congress: IAPRS, Vol.XXXV, part B3*, 2004.

[5] M. F. Tappen, W. T. Freeman, and E. H. Adelson, "Recovering Intrinsic Images from a Single Image.," *IEEE Trans. Pattern Anal. Mach. Intell.*, vol. 27, no. 9, pp. 1459–1472, 2005.

[6] J. J. Yoon, C. Koch, and T. J. Ellis, "ShadowFlash: an approach for shadow removal in an active illumination environment.," in *BMVC* (P. L. Rosin and A. D. Marshall, eds.), British Machine Vision Association, 2002.

[7] S. M. Smith and J. M. Brady, "SUSAN – A New Approach to Low Level Image Processing," *Int. J. Comput. Vision*, vol. 23, no. 1, pp. 45–78, 1997.

[8] M. Stokes, M. Anderson, S. Chandrasekar, and R. Motta, "A Standard Default Color Space for the Internet – sRGB, Version 1.10," 1996. `http://www.w3.org/Graphics/Color/sRGB`.

[9] A. Olmos and F. A. A. Kingdom, "McGill Calibrated Colour Image Database," 2004. `http://tabby.vision.mcgill.ca/`.

[10] G. Finlayson, M. Drew, and B. Funt, “Spectral sharpening: sensor transformations for improved color constancy,” *J. Opt. Soc. Am. A*, vol. 11, no. 5, pp. 1553–1563, 1994.